nature structural & molecular biology

The mechanism of pentabromopseudilin inhibition of myosin motor activity

Roman Fedorov[1], Markus Böhl[2], Georgios Tsiavaliaris[3], Falk K Hartmann[3], Manuel H Taft[3], Petra Baruch[1], Bernhard Brenner[4], René Martin[5], Hans-Joachim Knölker[5], Herwig O Gutzeit[2] & Dietmar J Manstein[1,3]

We have identified pentabromopseudilin (PBP) as a potent inhibitor of myosin-dependent processes such as isometric tension development and unloaded shortening velocity. PBP-induced reductions in the rate constants for ATP binding, ATP hydrolysis and ADP dissociation extend the time required per myosin ATPase cycle in the absence and presence of actin. Additionally, coupling between the actin and nucleotide binding sites is reduced in the presence of the inhibitor. The selectivity of PBP differs from that observed with other myosin inhibitors. To elucidate the binding mode of PBP, we crystallized the *Dictyostelium* myosin-2 motor domain in the presence of Mg^{2+}-ADP–*meta*-vanadate and PBP. The electron density for PBP is unambiguous and shows PBP to bind at a previously unknown allosteric site near the tip of the 50-kDa domain, at a distance of 16 Å from the nucleotide binding site and 7.5 Å away from the blebbistatin binding pocket.

Motor proteins belonging to the myosin family are among the best understood molecular machines. Myosin motor domains are accessible for analysis by an exceptionally wide range of experimental approaches, as they produce chemical, mechanical and spectroscopic changes during their active cycle. As a result, our understanding of the actomyosin system has now advanced to include detailed insights into the molecular mechanisms underlying the conversion of chemical energy into force and movement, which is catalyzed by the myosin motor domain. However, many questions remain to be solved for most of the myosin family members. The specific cellular functions and potential involvement in disease processes of many of the 39 members of the myosin family produced by the human body remain to be elucidated. What is evident already is that the role of myosins extends far beyond muscle contraction and the intracellular movement of vesicles. Their activities include roles in endocytosis, cytokinesis, nuclear anchoring, RNA polymerase I–dependent transcription and sensitization of transduction channels, and several members of the myosin family carry domains that are directly involved in signal transduction[1–6].

Small-chemical compounds that selectively alter the motor activity of individual myosin isoforms hold strong potential as tools for the analysis of complex biological processes and as therapeutics. In the process of performing assays aimed at the modulation of the β-adrenergic response of cardiomyocytes, we noticed that the marine natural product PBP inhibits myosin-dependent processes. The systematic name of PBP is 2,3,4-tribromo-5-(3,5-dibromo-2-hydroxyphenyl)-1*H*-pyrrole. PBP was originally isolated as an antibiotic from *Pseudomonas bromoutilis* with antitumor and phytotoxic activities and was shown to inhibit both 12- and 15-human lipoxygenase[7,8].

Further experiments using purified myosin revealed that PBP acts as a potent and reversible inhibitor of myosin ATPase and motor activities. To elucidate the inhibitory mechanism and to identify the PBP binding site, we characterized the effect of PBP on the kinetics of the ATPase cycle of myosins from several classes and organisms, examined its effect on the contraction of muscle fibers, and solved the crystal structure of PBP bound to the *Dictyostelium discoideum* myosin-2 motor domain. The structure shows that the inhibitor binds in a pocket close to the actin binding region at the tip of the 50-kDa domain and indicates myosin isoform–specific differences in the extent of PBP-mediated inhibition. Molecular modeling studies, predicting PBP to have particularly high affinity for vertebrate myosin-5a, are confirmed by the results of *in vitro* motility and ATPase assays. The selective inhibition of a myosin-5–dependent process in yeast shows the compound's potential as a tool in cell biological applications.

RESULTS

Kinetic mechanism of PBP-mediated inhibition of myosin

PBP inhibits the ATPase activities of a wide range of myosins with a distinct pattern of selectivity. Here we describe in detail the effects of PBP on the kinetic behavior of *D. discoideum* (*Dd*) myosin-5b. A wide range of spectroscopic signals can be measured with this myosin in the presence of PBP, and its kinetic properties have been described in detail[9]. To show the effect of PBP on the functional properties of other myosins, we include selected results

[1]Research Centre for Structure Analysis, OE8830, Hannover Medical School, 30623 Hannover, Germany. [2]Department of Biology, TU Dresden, Zellescher Weg 20b, 01217 Dresden, Germany. [3]Institute for Biophysical Chemistry, OE4350, Hannover Medical School, 30623 Hannover, Germany. [4]Institute for Molecular and Cellular Physiology, OE4210, Hannover Medical School, 30623 Hannover, Germany. [5]Department of Chemistry, TU Dresden, Bergstrasse 66, 01069 Dresden, Germany. Correspondence should be addressed to D.J.M. (manstein@bpc.mh-hannover.de).

Received 11 May 2008; accepted 2 December 2008; published online 4 January 2009; doi:10.1038/nsmb.1542

for rabbit skeletal muscle heavy meromyosin, chicken myosin-5a and recombinant *Dd* class 1 and class 2 myosins.

PBP decreases the maximum rate of basal and actin-activated myosin ATPase of all myosins tested. We obatined values for the rate of maximum ATP turnover (k_{cat}), the concentration of F-actin at which half-maximal activation is achieved (K_{app}) and the apparent second-order rate constant for actin binding ($k_{cat}/K_{app} = \Gamma$) from plots of steady-state actin-activated ATPase activity against the concentration of F-actin (**Fig. 1a**). Γ is a direct measure of the coupling efficiency between the actin and nucleotide binding sites. Plots of steady-state actin-activated ATPase activity against the concentration of PBP could be fitted to sigmoidal curves for each myosin (**Fig. 1b**).

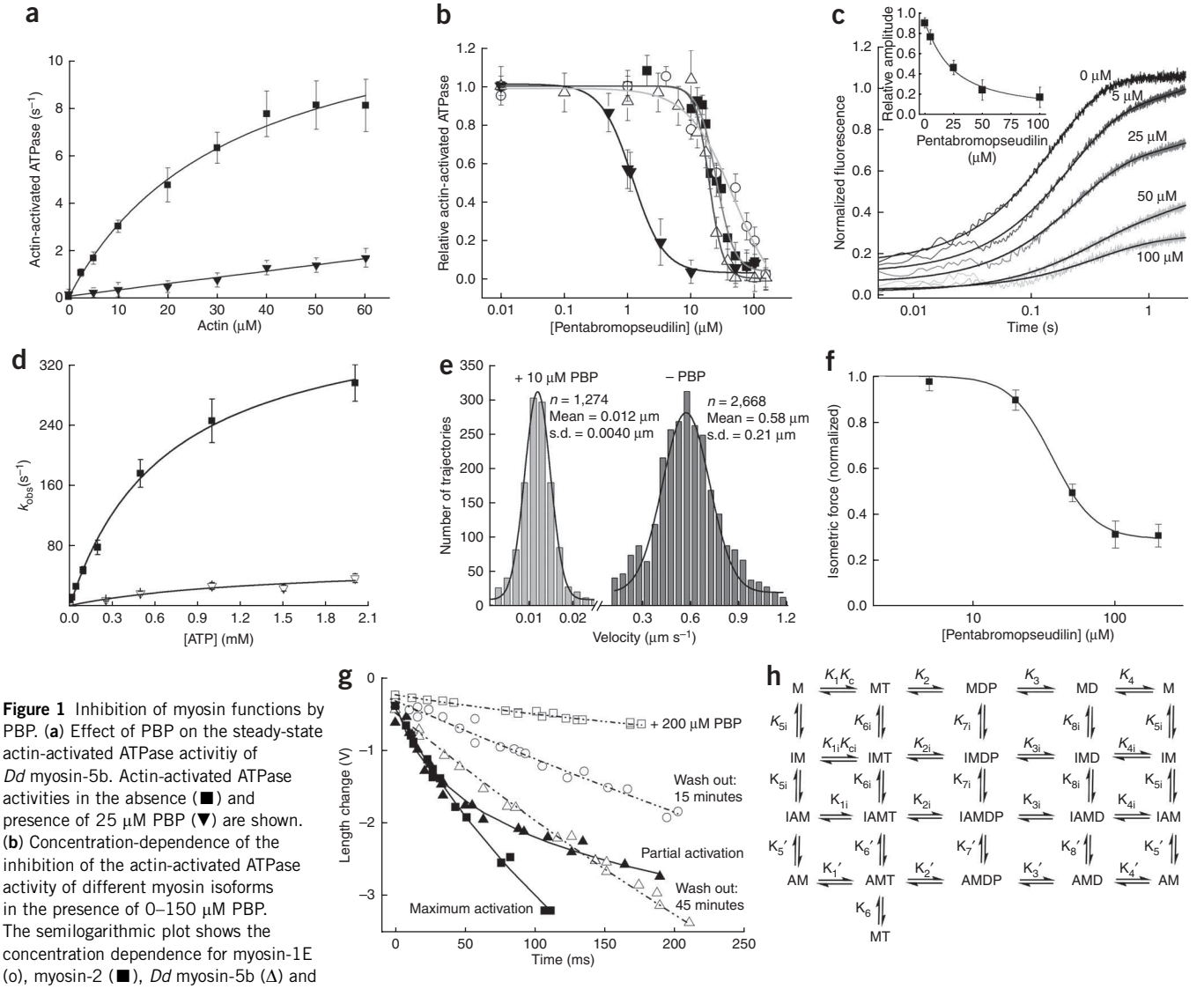

Figure 1 Inhibition of myosin functions by PBP. (**a**) Effect of PBP on the steady-state actin-activated ATPase activitiy of *Dd* myosin-5b. Actin-activated ATPase activities in the absence (■) and presence of 25 μM PBP (▼) are shown. (**b**) Concentration-dependence of the inhibition of the actin-activated ATPase activity of different myosin isoforms in the presence of 0–150 μM PBP. The semilogarithmic plot shows the concentration dependence for myosin-1E (○), myosin-2 (■), *Dd* myosin-5b (Δ) and chicken myosin-5a (▼). The concentrations of PBP required for half-maximal inhibition (IC_{50}) of the different myosin motors were determined from sigmoidal fits of the data. All parameters are summarized in **Table 1**. (**c**) Fluorescence transients obtained upon mixing 1 μM *Dd* myosin-5b with 10 μM mantATP in the absence and presence of 5 μM, 25 μM, 50 μM and 100 μM PBP. The concentration dependence of the amplitude of the fast phase is shown in the inset. (**d**) Rate constants for ATP binding and hydrolysis were determined by following the time-dependent changes in the intrinsic protein fluorescence of *Dd* myosin-5b. Addition of 25 μM PBP leads to a 14-fold reduction in the apparent second-order rate constant for ATP binding and a ten-fold reduction of the rate of ATP hydrolysis (**Supplementary Methods** online). (**e**) PBP-mediated inhibition of chicken myosin-5a in the *in vitro* motility assay. The histograms show the average sliding velocity of rhodamine-phalloidin–labeled actin filaments in the absence and presence of 10 μM PBP. Chicken myosin-5a moves actin filaments with an average velocity of 0.6 ± 0.05 μm s^{-1} (dark gray bars); addition of 10 μM PBP into the same flow cell decreases the average sliding velocity to 0.013 ± 0.002 μm s^{-1} (light gray bars). (**f**) Inhibition of steady-state level of isometric tension generated by skinned fibers of rabbit psoas muscle. Single fibers were first preincubated for 90 min with 200 mM PBP in relaxing solution before transfer to the activating solution containing the same PBP concentration. (**g**) Inhibition of unloaded shortening velocity by PBP. Each symbol represents the amplitude of imposed slack (length change) versus time required to take up the imposed slack by active shortening[48]. The slopes of the black curves give the velocity of unloaded shortening at maximum (■) and half-maximum (▲) Ca^{2+} activation in the absence of PBP. Changes in the slopes indicate that shortening velocity declines as shortening progresses in the absence of the inhibitor. The dotted lines show unloaded shortening after the fiber was incubated for 2 h in relaxing solution containing 200 μM PBP (□) and following wash out of PBP for 15 min (○) and 20 min (Δ). (**h**) Scheme describing the mechanism for PBP inhibition of basal and actin-activated myosin ATPase activity. The symbols used are as follows: A, actin; D, ADP; I, PBP; M, myosin; P, phosphate; T, ATP. Rate and equilibrium constants in the absence and presence of actin are distinguished by the use of italics versus bold type. Equilibrium constants are expressed as proceeding from left to right and above to below in this scheme. Error bars indicate s.d.

Table 1 Kinetic analysis of PBP inhibition

Steady-state parameters						
Myosin	Γ[a] ($\mu M^{-1}s^{-1}$)		Basal ATPase (s^{-1})		IC_{50} (μM)	
	–PBP	+PBP[b]	–PBP	+PBP[b]	–Actin	+Actin[c]
Dd myosin-1E[d]	0.17	n.d.	0.14 ± 0.03	0.018 ± 0.004	15.5 ± 1.5	49.5 ± 4.9
Dd myosin-2[d]	0.04	0.010	0.08 ± 0.01	0.015 ± 0.003	12.5 ± 1.2	24.4 ± 1.5
Oc myosin-2[e]	0.25	n.d.	0.06 ± 0.01	0.002 ± 0.001	9.8 ± 0.9	28.3 ± 5.4
Dd myosin-5b[d]	0.43	0.012	0.09 ± 0.01	0.007 ± 0.002	9.4 ± 1.7	19.3 ± 0.9
Gg myosin-5a[d]	11	n.d.	0.03 ± 0.01	0.006 ± 0.003	0.4 ± 0.2	1.2 ± 0.2

Transient parameters				
Dd myosin-5b (-PBP)		*Dd* myosin-5b (+PBP)		Units
k_{+1}	0.85 ± 0.04	k_{+1i}	0.29 ± 0.02	$\mu M^{-1}s^{-1}$
K_1k_{+c}	0.475 ± 0.02	$K_{1i}k_{+ci}$	0.033 ± 0.005	$\mu M^{-1}s^{-1}$
$k_{+2} + k_{-2}$	350 ± 20	$k_{+2i} + k_{-2i}$	37 ± 6	s^{-1}
k_{+3}	0.06 ± 0.01	k_{+3i}	0.035 ± 0.01	s^{-1}
k_{-4}	0.17 ± 0.01	k_{-4i}	0.11 ± 0.01	$\mu M^{-1}\ s^{-1}$
k_{+4}	0.92 ± 0.1	k_{+4i}	1.6 ± 0.2	s^{-1}
K_4	5.4 ± 0.9	K_{4i}	14.5 ± 2.5	μM
$\mathbf{K_1'k_{+6}}$	0.19 ± 0.01	$\mathbf{K_{1i}k_{-6i}}$	0.13 ± 0.01	$\mu M^{-1}\ s^{-1}$
$\mathbf{k_{+4}'}$	17.4 ± 1.7	$\mathbf{k_{+4i}}$	7.0 ± 0.8	s^{-1}
$\mathbf{k_{-4}'}$	4.0 ± 0.7	$\mathbf{k_{-4i}}$	5.7 ± 1.2	$\mu M^{-1}s^{-1}$
$\mathbf{K_4'}$	5.4 ± 2	$\mathbf{K_{4i}}$	1.23 ± 0.3	μM
$\mathbf{K_4'}/K_4$	1.0 ± 0.4	$\mathbf{K_{4i}}/K_{4i}$	0.08 ± 0.02	-
$\mathbf{k_{+6}}$	150 ± 10	$\mathbf{k_{-6i}}$	65 ± 4	s^{-1}

[a]Γ corresponds to the apparent second-order rate constant for actin binding (k_{cat}/K_{app}) that can be accurately determined from the initial slope of a plot k_{obs} against actin concentration at F-actin concentrations much smaller than K_{app}. [b]Measured in the presence of 25 μM PBP. [c]30 μM actin was added. [d]Single-headed motor domain construct. [e]Heavy meromyosin fragment. n.d., not determined; *Dd, D. discoideum*; *Gg, Gallus gallus*; *Oc, Oryctolagus cuniculus*.

The observed level of inhibition was greater than 50-fold for all myosins tested at saturating PBP concentrations. Among the myosins tested, chicken myosin-5a shows the most potent inhibition of actomyosin ATPase activity by PBP, with a half-maximal inhibitory concentration (IC_{50}) of 1.2 μM. Additionally, chicken myosin-5a is the only myosin with an apparent dissociation equilibrium constant for actin binding in the presence of ATP that is considerably lower than the maximum actin concentrations accessible (K_{app} = 1.4 μM). Therefore, the IC_{50} values in the presence of actin shown in **Table 1** define lower estimates for the other myosins. We also observed a sigmoidal dependence on the concentration of PBP for basal ATPase activity. Most myosins tested showed two- to three-fold lower IC_{50} values in the absence of actin than in its presence (**Table 1**).

To determine the exact mode of action of PBP, we carried out transient kinetic measurements with *Dd* myosin-5b. Results were interpreted according to the scheme shown in **Figure 1**, which describes mechanisms for the PBP-mediated inhibition of basal and actin-activated myosin ATPase activity. The major transient kinetics results obtained for *Dd* myosin-5b are summarized in **Table 1**. We used 2′(3′)-O-(*N*-methylanthraniloyl)-ATP (mantATP) and 2′(3′)-O-(*N*-methylanthraniloyl)-ADP (mantADP) for the initial characterization of the effect of PBP on nucleotide binding[10]. Addition of PBP to myosin motor domain constructs led to a marked loss in the rate and the amplitude of the mantATP-induced signal change. The observed transients showed monophasic behavior in the absence of PBP and in the presence of saturating concentrations of the inhibitor. At intermediate concentrations, we observed biphasic behavior, where the fast phase corresponds to binding of mantATP to M and the slow phase to mantATP binding to IM (**Fig. 1c**). The change in amplitude of the fast phase with increasing PBP concentrations shows an inverse hyperbolic dependence and gives an IC_{50} value of approximately 15 μM (**Fig. 1c**, insert). The presence of 50 μM PBP leads to an approximately three-fold reduction in the apparent second-order rate constants for mantATP binding from 0.85 $\mu M^{-1}\ s^{-1}$ to 0.29 $\mu M^{-1}\ s^{-1}$ (k_{+1}, k_{+1i}), whereas for mantADP binding (k_{-4}, k_{-4i}) we observed a less than two-fold decrease from 0.17 $\mu M^{-1}\ s^{-1}$ to 0.11 $\mu M^{-1}\ s^{-1}$ (**Supplementary Fig. 1a,b** online). The rate of mantADP release increased from 0.92 s^{-1} (k_{+4}) to 1.60 s^{-1} (k_{+4i}). The calculated dissociation equilibrium constants K_4 (5.4 μM) and K_{4i} (14.5 μM) indicate a three-fold reduction in the affinity of *Dd* myosin-5b for ADP in the presence of PBP (**Table 1**).

To determine rates of ATP binding and hydrolysis, we used the time-dependent change in the intrinsic protein fluorescence that follows the addition of excess ATP to *Dd* myosin-5b. We obtained a maximum rate of ATP hydrolysis ($k_{+2} + k_{-2}$) of 350 s^{-1} for *Dd* myosin-5b. The addition of 25 μM PBP led to a ten-fold reduction in the rate of ATP hydrolysis, and the apparent second-order rate constant for ATP binding slowed from 0.475 $\mu M^{-1}\ s^{-1}$ (K_1k_{+c}) to 0.033 $\mu M^{-1}\ s^{-1}$ ($K_{1i}k_{+ci}$) (**Fig. 1d**). To gain more information about the steps affected by PBP binding, we performed single-turnover experiments with *Dd* myosin-5b using mantATP as substrate (**Supplementary Fig. 1c**). In the absence of PBP, the time evolution of the reaction could be separated in three phases: an initial rise in mant fluorescence corresponding to binding of mantATP, a short, plateau phase determined by the rate of the conformational change that follows mantATP binding, and a drop in mant fluorescence corresponding to release and rebinding of mantADP ($k_{-4} + k_{+4}$). All three phases were extended in the presence of PBP. We interpret the extension of the plateau phase in the presence of PBP as the consequence of both slower mantATP hydrolysis and increased mantADP affinity. Single- and multiple-turnover experiments using ATP as substrate and measuring the release of inorganic phosphate[11] (P_i) indicate that that P_i release is

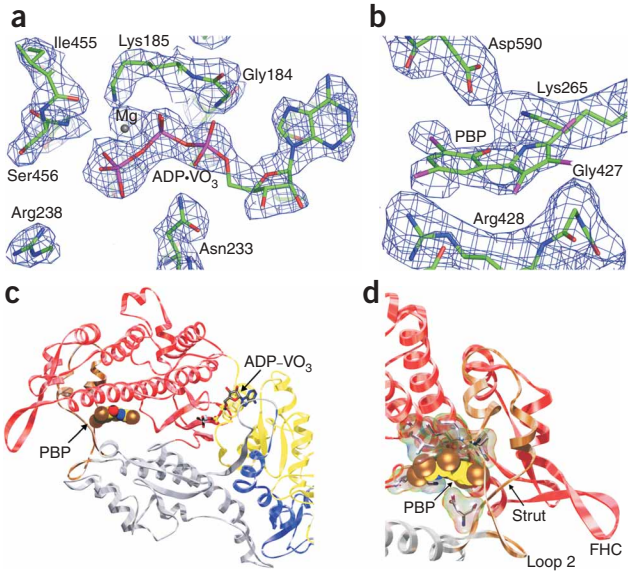

Figure 2 Structure of the myosin-2 motor domain in complex with PBP and Mg^{2+}-ADP–*meta*-vanadate. (**a**) Sections of the $2F_o - F_c$ electron density omit map showing the Mg^{2+}-ADP–*meta*-vanadate binding site and (**b**) the PBP binding site. The map was calculated using the final model of the myosin-2 motor domain with inhibitor and substrate omitted. The map was contoured at 1.0 σ. (**c**) Overall view of the myosin motor domain in ribbon representation. PBP is shown in spheres mode and nucleotide in stick representation. Yellow, 25-kDa domain; red, upper 50-kDa domain; gray, lower 50-kDa domain, blue, 20-kDa domain. The FHC loop, strut loop, loop 2 and the connecting helix-loop-helix motif are shown in light brown. (**d**) Close-up view of the PBP binding site. Selected residues interacting with PBP are shown in stick and van der Waals surface representation. The color scheme is the same as in **c**.

the rate-limiting step for *Dd* myosin-5b basal ATPase activity. Under multiple-turnover conditions, ADP release becomes the rate-limiting step (**Supplementary Fig. 1d**). In the presence of PBP, actin seems to increase the affinity of *Dd* myosin-5b for ADP rather than reducing it, whereas P_i release is not greatly affected (**Table 1**).

The rate of ATP binding to pyrene-labeled actomyosin was monitored by observing the exponential 20% increase in pyrene fluorescence as the complex dissociates upon addition of excess ATP. At lower ATP concentrations and in the absence of PBP, the observed rate constants increased linearly up to 50 μM ATP, giving a second-order rate binding constant of 0.19 μM^{-1} s^{-1} ($\mathbf{K_1'k_{+6}'}$).

Initial experiments showed only minor PBP-induced changes in the rate of the ATP-induced dissociation for the complex. This led us to question whether ATP-induced dissociation is more potently inhibited by PBP in the presence of ADP. Preincubation of the actomyosin complex with PBP and 5 μM ATP, followed by aging of the reaction mixture to allow formation of the IAMD complex, indeed led to a larger drop in the observed rates of ATP-induced dissociation of the complex. Owing to the presence of nucleotide-free and ADP-bound states under these conditions, the reaction shows biphasic behavior both in the absence and the presence of 50 μM PBP (**Supplementary Fig. 1e**). The initial fast phase corresponds to the binding of ATP to the nucleotide-free complex, and the second phase is determined by the dissociation of ADP from the AMD or IAMD complex. PBP affects the amplitudes and rate constants observed for both phases. Analysis of the fast phase indicates a 30% reduction in the second-order rate constant for ATP binding to IAM ($\mathbf{K_{1i}k_{-6i}}$) to 0.13 μM^{-1} s^{-1}. Addition of high ADP concentrations leads to monophasic dissociation reactions, with the observed rates of ATP-induced dissociation directly corresponding to the ADP dissociation rate from AMD ($\mathbf{k_{+4}'}$ = 17.4 s^{-1}) or IAMD ($\mathbf{k_{+4i}}$ = 7.0 s^{-1}) (**Supplementary Fig. 1f**). The total amplitude of the change in pyrene fluorescence is not affected by the presence of PBP, indicating that PBP does not prevent the formation of the strongly bound state.

The apparent second-order rate constants for ADP binding to acto-myosin-5b ($\mathbf{k_{-4}'}$, $\mathbf{k_{-4i}}$) were determined by monitoring the increase in mant fluorescence upon the addition of increasing concentrations of the fluorescent analog to acto-myosin-5b. The observed rate constants for the exponential increase in fluorescence were linearly dependent on mantADP concentration in the range of 1 μM to 30 μM (data not shown). The slopes of the straight lines fitted to the data gave values of 4.0 and 5.7 μM^{-1} s^{-1} for $\mathbf{k_{-4}'}$and $\mathbf{k_{-4i}}$, respectively. The dissociation equilibrium constant for mantADP binding to acto-myosin-5b in the presence of PBP ($\mathbf{K_{4i}}$) was calculated from $\mathbf{k_{+4i}}$ / $\mathbf{k_{-4i}}$ and corresponds to 1.23 μM. In the presence of 50 μM PBP, actin increases the affinity of ADP for *Dd* myosin-5b more than 12-fold, as indicated by the ratio of $\mathbf{K_{4i}}$ / K_{4i} (**Table 1**).

To demonstrate that the inhibitor exercises an allosteric effect on the open-closed transition of the nucleotide binding pocket, we used a *Dd* myosin-2 motor domain construct retaining a single tryptophan residue at position 501 (Trp501)[12]. The fluorescence emission intensity from Trp501, located at the distal end of the relay helix, is sensitive to the open-closed transition of the nucleotide binding pocket[13]. (**Supplementary Fig. 2** online).

PBP-mediated inhibition of myosin motor activity

To examine directly the inhibition of myosin motor activity by PBP, we performed *in vitro* motility assays and measured the effect of the inhibitor on the contraction of skinned muscle fibers. For the *in vitro* motility assays described here, we used chicken myosin-5a, which shows the full extent of inhibition at PBP concentrations below 10 μM in the *in vitro* motility assay. Under standard assay conditions, chicken myosin-5a moves F-actin with an average velocity of 600 nm s^{-1}. Addition of 10 μM PBP reduced the average sliding velocity approximately 50-fold to 13 nm s^{-1}, without reducing the number of moving filaments (**Fig. 1e**). These results show that myosin heads can still interact productively with F-actin in the presence of PBP, albeit at strongly reduced rates. PBP-mediated inhibition is reversible, as motile activity is almost completely recovered within minutes after wash-out of the inhibitor.

Next, we examined the ability of PBP to decrease tension generation by actively contracting fast skeletal muscle fibers. In the presence of 100 μM PBP, we observed a three-fold reduction in the steady-state level of isometric tension generated by skinned fibers of rabbit psoas muscle. **Figure 1f** shows the steady-state level of isometric tension as a function of the PBP concentration. The apparent IC_{50}, obtained from a sigmoidal fit to the data, corresponds to 25 μM for this skeletal muscle myosin-2–dependent process. Large PBP-mediated effects are observed for the velocity of unloaded shortening. Maximum inhibition was reached after equilibration of fibers for 2 h in relaxing solution with 200 μM PBP. Superposition of unloaded shortening at different degrees of Ca^{2+} activation and in the presence of different inhibitor concentrations reveals that, in the presence of inhibitor, unloaded shortening is slowed down in both the initial and late phases of shortening (**Fig. 1g**). The effects of PBP on tension redevelopment and stiffness-speed profiles[14] are shown in **Supplementary Fig. 3** online. The observed PBP-induced reductions in k_{TR} and isometric

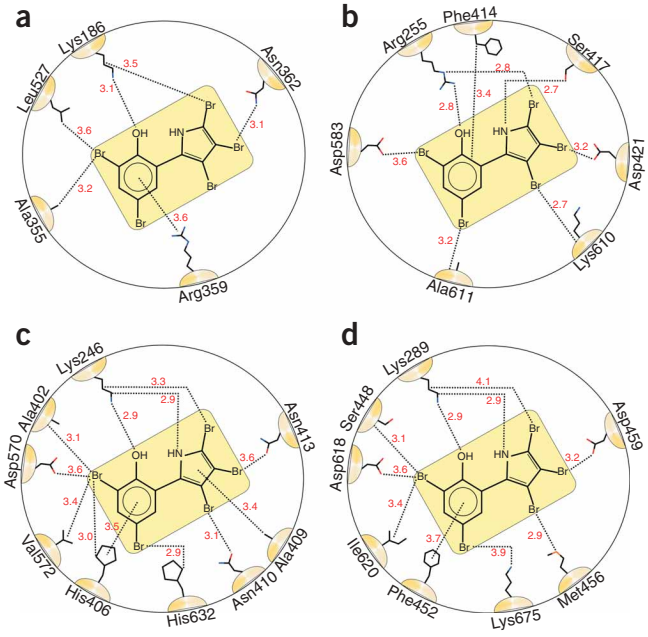

Figure 3 PBP binding site and contact residue conservation for different myosin isoforms. Myosin residues interacting with PBP are shown as predicted by molecular modeling for *Dd* myosin-1E (**a**), *Sc* Myo2 (**b**), *Gg* myosin-5a (**c**) and *Dd* myosin-5b (**d**).

force, minor changes in stiffness and slower shortening during the late phase are consistent with a slower transition into force-generating states. A slow initial phase of shortening is consistent with the observed reductions in the rates for ADP release and ATP-induced dissociation in the presence of PBP.

Identification of the PBP binding site

To identify the PBP binding site, we crystallized the *Dd* myosin-2 motor domain Mg^{2+}-ADP–*meta*-vanadate complex in the absence and presence of PBP. We solved the structures by molecular replacement and refined them to 2.3-Å and 2.8-Å resolution, respectively. The overall fold of the motor domain in both structures is similar to that reported for the pre-powerstroke conformation[15]. In contrast to the geometries of the *ortho*-vanadate–ADP complexes, where the vanadate moiety has a trigonal bipyramidal conformation, the *meta*-vanadate complex shows tetrahedral symmetry, and the distance between the vanadium atom and the β-γ–bridging oxygen is 1.8 Å instead of 2.1 Å. The *meta*-vanadate ion thus fully replaces the position of γ-phosphate, forming a covalent bond with the β-phosphate moiety of ADP (**Fig. 2a**). Therefore, the nucleotide *meta*-vanadate complex at the active site and the overall myosin motor domain structure most closely resemble those of ATP and the ATP-bound state.

The electron density for PBP is unambiguous and shows the inhibitor to bind in a pocket close to actin binding residues and located 16 Å away from the nucleotide binding site. PBP takes a conformation where the phenyl and pyrrole ring systems are bent by 12° out of plane and twisted by 20° against each other (**Fig. 2b–d**). The total protein surface area in contact with PBP comprises 255 $Å^2$, and both polar and apolar residues contribute to the binding of PBP. The inner face of this PBP binding pocket is formed by helix 13 (Lys265–Val268) and helix 21 (Val411–Leu441) from the 50-kDa upper domain (U50). The outer face is contributed by the strut loop (Asn588–Gln593) and loop 2 (Asp614–Thr629), which are connected by the helix-loop-helix motif that covers parts of the cleft and the U50 in a lid-like fashion. The PBP binding pocket has a large opening toward the exterior and the large cleft that is surrounded by residues from loop 2, helix 21, helix 29 (Val630–Glu646) and the loop connecting β7 (Ile253–Leu261) with helix 13. Additionally, a smaller access channel is located between loop 2 and the strut loop. The α-carbon atoms in the Mg^{2+}-ADP–*meta*-vanadate complex structures with and without bound PBP superimpose with an r.m.s. deviation of 0.695 Å, indicating that the myosin motor domain does not undergo any major conformational changes upon binding of PBP, except for local changes directly involved in the coordination of the inhibitor. The importance of loop 2 and the strut loop for coupling between the actin and nucleotide binding sites and cleft closure were demonstrated by mutagenesis studies[13]. In particular, it was shown that removal or repositioning of Asp590, a residue that is directly involved in the coordination of PBP, destroys strong binding of *Dd* myosin-2 to F-actin[16].

Binding of PBP requires several rearrangements of residues inside and near the binding pocket, as described in **Supplementary Figure 4** online. On the basis of the structure of the *Dd* myosin-2 motor domain with bound PBP, we performed molecular modeling studies to elucidate the structural basis of the observed differences in PBP binding to myosins from different classes. The results for the modeling of the complexes formed with class 1 and class 5 myosins are shown in **Figure 3**. The interaction of a basic residue corresponding to Lys265 in myosin-2 with the hydroxyl group of PBP is a common feature of all complexes. However, the total number of interactions and their strength is predicted to vary considerably between individual myosins. *Dd* myosin-2 forms four hydrogen bonds and six weaker van der Waals interactions with PBP (4/6). The numbers of predicted interactions with PBP are 12 (6/6) for chicken myosin-5a, 8 (6/2) for *Saccharomyces cerevisiae* Myo2, 9 (5/4) for *Dd* myosin-5b, and 6 (3/3) for *Dd* myosin-1E. In agreement with these results, the steady-state ATPase of chicken myosin-5a showed a much larger decrease in ATPase activity than was observed for the other myosins. Additionally, the predicted number of interactions correlates well with the IC_{50} shown in **Table 1**.

Inhibition of myosin-5–dependent cellular processes

To test the specific inhibition of myosin-5 function in a cellular context, we exposed *S. cerevisiae* cells to concentrations of 100–500 nM PBP. *S. cerevisiae* (*Sc*) has five myosin heavy-chain genes encoding a class 2 myosin (Myo1), two class 1 myosins (Myo3 and Myo5) and the class 5 myosins Myo2 and Myo4. Myo2 has a crucial role in polarized distribution of mitochondria and is required for retention of newly inherited mitochondria in yeast cells during cell division[17,18]. Myo4 is required for mRNA transport and facilitates movement of endoplasmic reticulum tubules into the growing bud[19]. Myo4-null mutants are viable and have no detectable phenotype[20]. Deletion of the *myo3* and *myo5* genes, encoding class 1 myosins, leads to severe defects in growth and actin cytoskeletal organization[21]. Severe growth defects are also observed upon depletion of the class 2 myosin Myo1 (ref. 22). Thus, Myo2-dependent changes in the morphology of mitochondria should be readily distinguishable from the defects in cell growth, actin cytoskeletal organization and cytokinesis expected from the inhibition of other yeast myosins. Additionally, homology modeling of Myo2 in complex with the inhibitor predicts that PBP is a potent inhibitor of Myo2 function, with six hydrogen bonds contributing to the interaction (**Fig. 3b**). The interaction pattern between the protein matrix and the inhibitor is basically identical to that of *Dd* myosin-2, but most side chain replacements contribute to stronger

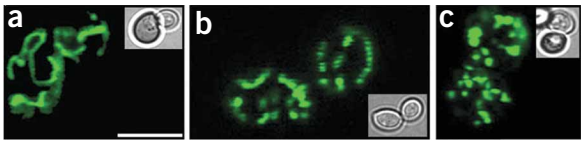

Figure 4 *Sc* Myo2p-dependent changes in mitochondrial morphology. In yeast cells, the class-5 myosin Myo2 is responsible for the distribution of mitochondria between mother and daughter cells during cytokinesis and has been shown to affect mitochondrial morphology during interphase. (**a**) Wild-type yeast cells. (**b**) Myo2-depleted cells. (**c**) The phenotype of Myo2-depleted cells is phenocopied by exposure of wild-type cells to 500 nM PBP. Insets show the same cells viewed under transmitted light. Scale bar: 5 μm.

binding. Replacement of *Dd* myosin-2 residues Leu431 and Lys265 with Asp421 and Arg255 in Myo2 leads to the formation of two additional hydrogen bonds, and replacement of Ala424 with Phe414 increases the efficiency of the hydrophobic interaction between the corresponding part of the binding pocket and the inhibitor. The replacement of *Dd* myosin-2 residue Arg428 with an alanine residue leads to the loss of a van der Waals interaction but does not affect the local structure of the binding pocket.

To facilitate the visual inspection of mitochondrial morphology, we used cells transfected with an expression vector for the production of mitochondria-targeted GFP[23] (**Fig. 4a**). We used a yeast mutant strain with *myo2* expression under the control of the $TetO_7$ promoter as a control[24]. Repression of the $TetO_7$ promoter by the addition of 10 μg ml^{-1} deoxycycline to the culture medium of this strain led to an apparent fragmentation of mitochondria (**Fig. 4b**). We saw similar phenotypic changes when wild-type cells were exposed to 500 nM PBP for 12 h (**Fig. 4c**). At lower concentrations, the phenotype was less severe, and at 100 nM PBP the mitochondrial morphology closely resembled that of untreated wild-type cells. Yeast cells exposed to 500 nM PBP showed normal cytokinesis and similar long-term growth kinetics as the wild-type control cultures, indicating that inhibition is Myo2 specific.

DISCUSSION

Our results show that the halogenated pseudilin derivative PBP acts as allosteric inhibitor of myosin function. PBP binds in a pocket close to actin binding residues, open to the exterior and to the large cleft. Blebbistatin, the other structurally well-characterized inhibitor of myosin motor activity, binds to a site 7.5 Å away from the PBP pocket[25]. Blebbistatin is thought to inhibit P_i release by sitting like a wedge in a hydrophobic pocket at the base of the large cleft. This prevents complete closure of the cleft and thereby stabilizes the ADP-P_i transition state[25]. A similar stabilization of a product complex with low actin affinity has been observed with BTS, a specific inhibitor of fast skeletal muscle myosin-2 (ref. 26). Transient kinetic analysis of *Dd* myosin-5b showed that PBP affects both reaction steps leading to weak and strong actin binding states and indicates that other myosins are affected in a similar way by PBP.

The addition of ATP to the IAM complex leads to the formation of the IAMT complex ($\mathbf{K_{1i}k_{Ci}}$), followed by dissociation of actin and formation of the IMT complex ($\mathbf{k_{-6i}}$) (see the scheme in **Figure 1h**). These steps are 1.5- and 4-fold slower in the presence of PBP. The reaction proceeds with the hydrolysis step ($k_{+2i} + k_{-2i}$) leading to the formation of the ternary IMDP complex. The hydrolysis step shows the largest PBP-induced change, with a ten-fold reduction in the rate of the process. Hydrolysis is followed by rapid reassociation with actin, leading to the formation of the IAMDP complex ($\mathbf{k_{+7i}}$). The pentanary complex decomposes in the direction of phosphate release ($\mathbf{k_{+3i}}$). Both P_i release and the preceding step are not substantially affected by PBP. The cycle is closed with the formation of the IAM complex following the dissociation of ADP from the IAMD complex ($\mathbf{k_{+4i}}$). This step is the rate limiting step for the steady-state actin-activated ATPase activity of *Dd* myosin-5b in the presence of saturating concentrations of PBP.

The PBP-induced changes in multiple rate constants lead to an increase of the actin-activated ATP-cycle time and shift the ratio of the time spend per cycle in strong and weak binding states. The slower movement of actin filaments in the *in vitro* motility assay observed with myosins from different classes, and the myosin-2–dependent reduction in unloaded shortening velocity in single-fiber experiments, indicate that steps associated with ADP release and ATP-induced dissociation of actomyosin are slowed down in the presence of PBP[27]. Additionally, the decrease in isometric tension generation observed in single-fiber experiments indicates a PBP-induced redistribution in favor of cycle-time spend in non–force-generating states, at least for skeletal muscle myosin-2–dependent processes. In the case of class-5 myosins, which show weaker coupling between actin binding and ADP release, the addition of PBP leads to a similar extension of total cycle time but with a more dominant contribution of cycle-time spend in force-generating states. In the case of *Dd* myosin-5b, the coupling ratio ($\mathbf{K_4'}$ / K_4) equals unity and becomes reversed in the presence of PBP ($\mathbf{K_{4i}}$ / $K_{4i} = 0.08$). As a consequence, actin increases the affinity of *Dd* myosin-5b for ADP ($\mathbf{K_{4i}} = 1.23$ μM), and strong binding states become dominant under experimental conditions where ADP concentrations are not kept low.

Changes in the actin interface upon closure of the large cleft between U50 and L50, which are necessary for formation of the strongly bound myosin states on actin and efficient release of ATP-hydrolysis products, involve large rearrangements of residues that are located near the PBP binding pocket[28,29]. The rearrangements are in turn coupled to significant movements of nucleotide binding loop structures by a distortion of the central β-sheet. The switch-1 loop preceding β6, the switch-2 loop following β5 and the P-loop following β4 undergo large conformational changes between the nucleotide-free and the catalytically competent structures. Cleft closure is thus coupled to the opening of the nucleotide binding pocket and the disruption of interactions that stabilize γ-phosphate binding, the coordination of the Mg^{2+} ion and, thereby, ADP binding[30,31]. Although the PBP binding site is formed in part by residues that are implicated in these movements, the size and binding mode of PBP are not compatible with a mechanism were PBP interferes with cleft closure. Furthermore, the results of our kinetic, motility and tension measurements show conclusively that PBP does not block the formation of a strongly bound actomyosin complex, and molecular modeling shows that the interactions of PBP with residues in the U50 are not affected by closure of the cleft. The effects of changes in the strut loop and loop 2 are more difficult to predict; however, even here, cleft closure does not necessarily lead to a disruption of the interactions with PBP. This is supported by our experimental result. The observed changes in IC_{50} values for basal and actin-activated ATPase activities indicate that the formation of a rigor-state actomyosin complex results in a less than ten-fold reduction in PBP binding affinity.

Our results using yeast as a model system to block a myosin-5–dependent process show that PBP has potential as a tool for cell-motility studies. PBP readily permeates membranes and showd a clearly distinct selectivity for myosin isoforms. It is not a specific inhibitor of all myosins belonging to class 5, but it strongly inhibits the function of individual members of class 5, such as vertebrate myosin-5a. An important aspect of the characterization of PBP is its role as a

lead compound for the development of more specific effectors of myosin function. The residues involved in PBP binding are only moderately conserved between the members of the different myosin classes, as reflected by the observed differences in the IC_{50} values for the myosin isoforms characterized in this study. Moreover, our results show that isoform-specific variations in the extent of PBP-mediated inhibition can be predicted at least in trend. The continuity of the PBP binding pocket with the 50-kDa cleft indicates that the site can accommodate much bulkier compounds. As the affinity and specificity of drug-enzyme interactions tends to increase with their area of interaction, the structure-based design of compounds that extend into the cleft promises to improve their selectivity for individual myosin isoforms. Highly selective effectors of specific myosin isoforms have a wide range of potential therapeutic applications in the treatment of diseases including cancer, heart failure and malaria[32–34]. Furthermore, the structural and functional framework provided by our results can be used to design compounds that, upon binding, induce specific functional changes in the myosin motor that are distinct from those observed with PBP.

METHODS

Protein preparation. We purified His_6-tagged motor domain constructs of *Dd* myosin-1E, myosin-2 and myosin-5b comprising amino acids 1–698, 1–765 and 1–839 respectively, by Ni^{2+}-chelate–affinity chromatography[35]. Myosin-5a heavy meromyosin from chicken brain was provided by T. Scholz (Hannover Medical School, Germany). Rabbit fast skeletal muscle heavy meromyosin (HMM), F-actin and pyrene-labeled F-actin were prepared as described[36–38].

Synthesis of PBP. We synthesized PBP using a silver (I)–catalyzed cyclization to the pyrrole ring system[39].

Steady-state kinetics. We measured basal and actin-activated Mg^{2+}-ATPase activities using the NADH-coupled assay described previously[40]. PBP was added to the reaction mixture in the absence of nucleotide and incubated for 20 min, before the reaction was started by the addition of ATP. Tests of the inhibitory potency of pseudilin and halogenated pseudilins were performed with HMM prepared from rabbit skeletal muscle myosin-2. Each reaction mixture including the controls contained 2.5% (v/v) DMSO, which was used as solvent for the small organic compounds. Reactions containing HMM (0.01 mg ml^{-1}), assay buffer (50 mM KCl, 5 mM $CaCl_2$, 25 mM Tris-HCl, pH 7.5) and 25 μM of the respective inhibitor were preincubated for 20 min at 37 °C, and the reaction was started by the addition of 50 μM ATP. We terminated reactions after 20 min at 37 °C by the addition of Biomol Green (Biomol). The amount of dye formed after 20 min of color development at room temperature (20–23 °C) was determined by absorption measurements at 640 nm with a Tecan Infinite microplate reader (Crailsheim). Data were corrected for inhibitor absorption at 640 nm and expressed as relative myosin ATPase activity (as a percentage of the control).

Transient kinetics. We performed stopped-flow experiments with PiStar (Applied Photophysics) and Hi-Tech SF61 (TgK Scientific Limited) spectrophotometers using procedures and kinetic models described previously[41]. Tryptophan fluorescence was excited at 296 nm and detected after passing through a WG320 cut-off filter. Pyrene and mant fluorescence were excited at 365 nm and detected after passing through a KV 389 nm cut-off filter. Data analysis was performed with software provided by TgK Scientific Limited, Applied Photophysics, and with Origin 7.0 (Originlab Corporation).

***In vitro* motility assay.** We performed actin-sliding motility assays at 25 °C using an Olympus IX81 (Olympus) inverted fluorescence microscope as described previously[42]. Equine cytochrome C was used as blocking agent instead of BSA. Average sliding velocities were determined from the Gaussian distribution of automatically tracked actin filaments using DiaTrack 3.0 (Semasopht). Additional data analysis was performed with Origin 7.0.

Crystallization and data collection. We grew crystals of the motor domain construct M761-c14 carrying an N-terminal His_7 tag and a C-terminal SSB tag (LARIEEAREQRLESNEPPMDFDDDIPF) (ref. 43) in the presence of sodium *meta*-vanadate and ADP or sodium *meta*-vanadate, ADP and PBP at 4 °C using the hanging drop geometry. Equal amounts (2 μl) of complex solution and reservoir solution were mixed, the latter containing 50 mM HEPES pH 7.4, 140 mM NaCl, 11% (w/v) PEG8000, 2% (v/v) MPD, 5 mM $MgCl_2$, 5 mM DTT and 1 mM EGTA. Before diffraction data collection, we soaked crystals for 5 min at 4 °C in a cryoprotection solution containing reservoir solution supplemented with 25% (v/v) ethylene glycol, 2 mM sodium *meta*-vanadate and 2 mM ADP. Subsequently, crystals were flash-cooled in liquid nitrogen. We collected diffraction data for the myosin-2 motor domain Mg^{2+}-ADP–*meta*-vanadate complex at EMBL beamline X11 at the DORIS storage ring, DESY, Hamburg. Diffraction data for the complex with PBP were collected in house using an X8PROTEUM system equipped with cryosystem, κ-goniometer and CCD detector and processed with PROTEUM2 software (Bruker AXS). We solved the structures using $C222_1$ data by the molecular replacement method using PDB 1VOM as the initial model (**Table 2**).

Table 2 Data collection and refinement statistics

	Myosin-2–ADP–VO_3–PBP	Myosin-2–ADP–VO_3
Data collection		
Space group	$C222_1$	$C222_1$
Cell dimensions		
a, *b*, *c* (Å)	89.8, 150.5, 154.6	89.4, 147.2, 153.8
Resolution (Å)	20.0–2.8	20.0–2.1
R_{sym} (%)	8.8 (40.4)*	5.8 (40.8)
$I / \sigma I$	10.9 (2.4)	24.4 (5.0)
Completeness (%)	98.2 (95.5)	98.2 (98.5)
Redundancy	5.2 (4.0)	9.5 (6.9)
Refinement		
Resolution (Å)	8.0–2.8	8.0–2.3
R_{work} / R_{free} (%)	21.7 / 26.5	22.5 / 27.5
No. reflections working / test set	22,214 / 1,178	43,111 / 2,268
No. atoms		
Protein	6,240	5,535
Ligands/ions	48 / 1	31 / 1
Water	477	508
B-factors (Å^2)		
Protein	41.9	42.7
Ligands/ions	31.3 / 31.2	30.8 / 28.9
Water	39.2	51.5
R.m.s. deviations		
Bond lengths (Å)	0.009	0.006
Bond angles (°)	1.4	1.3

Each data set was collected using a single crystal. *Values in parentheses are for highest-resolution shell.

Single-fiber mechanics. We isolated single fibers from bundles of chemically skinned fibers of the muscle psoas of rabbits, as described previously[44,45]. One end of the isolated fibers was attached to the lever of a modified moving coil galvanometer for length control, the other to a strain gauge force transducer (Akers). Overall fiber length was set such that sarcomere length was 2.4 μm. We measured sarcomere length by diffraction of a 633-nm helium-neon laser beam. Composition of relaxing and activating solutions were identical to our previous work[46,47]. Ionic strength of activating and preactivating solutions was adjusted to 170 mM and 50 mM for the solution to measure stiffness of relaxed fibers at 'low ionic strength'. Ionic strength was adjusted by addition of appropriate amounts of potassium propionate. Experimental temperature was set to 5 °C. Unloaded shortening was measured by the slack test[48].

Molecular modeling. We used the motor domain structures of *Dd* myosin-1E (PDB 1LKX) and chicken myosin-5a (PDB 1OE9) to model the complexes of class 1 and class 5 myosins with PBP. Initial models were created by inserting PBP coordinates from the superimposed myosin-2–PBP complex. Next,

molecular mechanics energy-minimization procedures were performed for PBP in the new protein environment using the CNS software suit[49]. The resulting structures were subjected to a more precise quantum chemical energy–minimization procedure, using *ab initio* DFT QM/MM calculations with the 6-31G* basis set of atomic orbitals and B3LYP hybrid functional. The quantum chemical calculations were performed using the PC GAMESS version developed by A. A. Granovsky (http://classic.chem.msu.su/gran/gamess/index.html) of the GAMESS (US) Quantum Chemistry package[50].

Myo2-dependent changes in mitochondrial morphology. Yeast strains producing mitochondria-targeted GFP were supplied by B. Westermann[23]. Repression of the $TetO_7$ promoter that controls *myo2* in one of the mutant strains was achieved by the addition of 10 μg ml^{-1} deoxycycline to the culture medium[24]. Cells were analyzed at the end of the logarithmic growth phase. Images were acquired using a LSM 510 confocal microscope (Carl Zeiss AG) using a 63× oil immersion objective and an ORCA camera (Hamamatsu Photonics GmbH) for bright-field imaging.

Accession codes. Protein Data Bank: Coordinates for the myosin-2 motor domain–ADP–*meta*-vanadate and myosin-2 motor domain–ADP–*meta*-vanadate–PBP complexes have been deposited with the accession codes 2JJ9 and 2JHR, respectively.

Note: Supplementary information is available on the Nature Structural & Molecular Biology website.

ACKNOWLEDGMENTS

We thank S. Fujita-Becker (Max-Planck-Institute for Medical Research, Heidelberg), B. Westermann (University of Bayreuth), T. Scholz, A. Schweda (Hannover Medical School) A. Malnasi-Csizmadia and M. Kovacs (Eötvös Lorand University, Budapest), and C.R. Bagshaw (University of Leicester) for reagents; M.A. Geeves for discussions; C. Thiel, C. Wassmann, Y. Henker and L. Litz for excellent technical assistance. We are grateful to the staff of beamline EMBL X11 at the DORIS storage ring of DESY for their support.

AUTHOR CONTRIBUTIONS

R.F. performed crystallization, structure determination and molecular modeling; M.B. performed the initial kinetic screening of the pseudilin derivatives and the yeast assays; G.T. supervised and codesigned the protein preparation, kinetic and *in vitro* motility assays, and performed the transient kinetic analysis with F.K.H. and M.H.T.; F.K.H. performed *in vitro* motility assays and steady-state analysis; M.H.T. performed transient kinetic experiments; P.B. crystallized the protein inhibitor complexes; B.B. designed and performed single-fiber experiments; R.M. synthesized PBP; H.-J.K. designed and supervised compound synthesis; H.O.G. designed and supervised the initial kinetic screening of PBP and the yeast assays; D.J.M. supervised kinetic analysis, crystallization and data collection, molecular modeling, *in vitro* motility analysis, advised on the design of the experiments, and wrote the manuscript with G.T., R.F., H.O.G., B.B. and H.-J.K.

Published online at http://www.nature.com/nsmb/
Reprints and permissions information is available online at http://npg.nature.com/reprintsandpermissions/

1. Sokac, A.M., Schietroma, C., Gundersen, C.B. & Bement, W.M. Myosin-1c couples assembling actin to membranes to drive compensatory endocytosis. *Dev. Cell* **11**, 629–640 (2006).
2. Arden, S.D., Puri, C., Au, J.S., Kendrick-Jones, J. & Buss, F. Myosin VI is required for targeted membrane transport during cytokinesis. *Mol. Biol. Cell* **18**, 4750–4761 (2007).
3. Zhang, H. *et al.* Myosin-X provides a motor-based link between integrins and the cytoskeleton. *Nat. Cell Biol.* **6**, 523–531 (2004).
4. Cavellan, E., Asp, P., Percipalle, P. & Farrants, A.K. The WSTF-SNF2h chromatin remodeling complex interacts with several nuclear proteins in transcription. *J. Biol. Chem.* **281**, 16264–16271 (2006).
5. van den Boom, F., Dussmann, H., Uhlenbrock, K., Abouhamed, M. & Bahler, M. The Myosin IXb motor activity targets the myosin IXb RhoGAP domain as cargo to sites of actin polymerization. *Mol. Biol. Cell* **18**, 1507–1518 (2007).
6. Weber, K.L., Sokac, A.M., Berg, J.S., Cheney, R.E. & Bement, W.M. A microtubule binding myosin required for nuclear anchoring and spindle assembly. *Nature* **431**, 325–329 (2004).
7. Ohri, R.V. *et al.* A Re(V)-catalyzed C-N bond-forming route to human lipoxygenase inhibitors. *Org. Lett.* **7**, 2501–2504 (2005).
8. Burkholder, P.R., Pfister, R.M. & Leitz, F.H. Production of a pyrrole antibiotic by a marine bacterium. *Appl. Microbiol.* **14**, 649–653 (1966).
9. Taft, M.H. *et al.* *Dictyostelium* myosin-5b is a conditional processive motor. *J. Biol. Chem.* **283**, 26902–26910 (2008).
10. Hiratsuka, T. Fluorescence properties of 2′ (or 3′)-O-(2,4,6-trinitrophenyl) adenosine 5′-triphosphate and its use in the study of binding to heavy meromyosin ATPase. *Biochim. Biophys. Acta* **453**, 293–297 (1976).
11. Webb, M.R. A continuous spectrophotometric assay for inorganic phosphate and for measuring phosphate release kinetics in biological systems. *Proc. Natl. Acad. Sci. USA* **89**, 4884–4887 (1992).
12. Malnasi-Csizmadia, A., Kovacs, M., Woolley, R.J., Botchway, S.W. & Bagshaw, C.R. The dynamics of the relay loop tryptophan residue in the *Dictyostelium* myosin motor domain and the origin of spectroscopic signals. *J. Biol. Chem.* **276**, 19483–19490 (2001).
13. Geeves, M.A., Fedorov, R. & Manstein, D.J. Molecular mechanism of actomyosin-based motility. *Cell. Mol. Life Sci.* **62**, 1462–1477 (2005).
14. Brenner, B., Yu, L.C., Greene, L.E., Eisenberg, E. & Schoenberg, M. Ca^{2+}-sensitive cross-bridge dissociation in the presence of magnesium pyrophosphate in skinned rabbit psoas fibers. *Biophys. J.* **50**, 1101–1108 (1986).
15. Dominguez, R., Freyzon, Y., Trybus, K.M. & Cohen, C. Crystal structure of a vertebrate smooth muscle myosin motor domain and its complex with the essential light chain: visualization of the pre-power stroke state. *Cell* **94**, 559–571 (1998).
16. Sasaki, N., Ohkura, R. & Sutoh, K. Insertion or deletion of a single residue in the strut sequence of *Dictyostelium* myosin II abolishes strong binding to actin. *J. Biol. Chem.* **275**, 38705–38709 (2000).
17. Boldogh, I.R., Ramcharan, S.L., Yang, H.C. & Pon, L.A. A type V myosin (Myo2p) and a Rab-like G-protein (Ypt11p) are required for retention of newly inherited mitochondria in yeast cells during cell division. *Mol. Biol. Cell* **15**, 3994–4002 (2004).
18. Itoh, T., Watabe, A., Toh, E.A. & Matsui, Y. Complex formation with Ypt11p, a Rab-type small GTPase, is essential to facilitate the function of Myo2p, a class V myosin, in mitochondrial distribution in *Saccharomyces cerevisiae*. *Mol. Cell. Biol.* **22**, 7744–7757 (2002).
19. Shepard, K.A. *et al.* Widespread cytoplasmic mRNA transport in yeast: identification of 22 bud-localized transcripts using DNA microarray analysis. *Proc. Natl. Acad. Sci. USA* **100**, 11429–11434 (2003).
20. Simon, V.R., Swayne, T.C. & Pon, L.A. Actin-dependent mitochondrial motility in mitotic yeast and cell-free systems: identification of a motor activity on the mitochondrial surface. *J. Cell Biol.* **130**, 345–354 (1995).
21. Goodson, H.V., Anderson, B.L., Warrick, H.M., Pon, L.A. & Spudich, J.A. Synthetic lethality screen identifies a novel yeast myosin I gene (*MYO5*): myosin I proteins are required for polarization of the actin cytoskeleton. *J. Cell Biol.* **133**, 1277–1291 (1996).
22. Lord, M., Laves, E. & Pollard, T.D. Cytokinesis depends on the motor domains of myosin-II in fission yeast but not in budding yeast. *Mol. Biol. Cell* **16**, 5346–5355 (2005).
23. Westermann, B. & Neupert, W. Mitochondria-targeted green fluorescent proteins: convenient tools for the study of organelle biogenesis in *Saccharomyces cerevisiae*. *Yeast* **16**, 1421–1427 (2000).
24. Mnaimneh, S. *et al.* Exploration of essential gene functions via titratable promoter alleles. *Cell* **118**, 31–44 (2004).
25. Allingham, J.S., Smith, R. & Rayment, I. The structural basis of blebbistatin inhibition and specificity for myosin II. *Nat. Struct. Mol. Biol.* **12**, 378–379 (2005).
26. Cheung, A. *et al.* A small-molecule inhibitor of skeletal muscle myosin II. *Nat. Cell Biol.* **4**, 83–88 (2002).
27. Nyitrai, M. *et al.* What limits the velocity of fast-skeletal muscle contraction in mammals? *J. Mol. Biol.* **355**, 432–442 (2006).
28. Reubold, T.F., Eschenburg, S., Becker, A., Kull, F.J. & Manstein, D.J. A structural model for actin-induced nucleotide release in myosin. *Nat. Struct. Biol.* **10**, 826–830 (2003).
29. Coureux, P.D. *et al.* A structural state of the myosin V motor without bound nucleotide. *Nature* **425**, 419–423 (2003).
30. Reubold, T.F., Eschenburg, S., Becker, A., Kull, F.J. & Manstein, D.J. A structural model for actin-induced nucleotide release in myosin. *Nat. Struct. Biol.* **10**, 826–830 (2003).
31. Coureux, P.D. *et al.* A structural state of the myosin V motor without bound nucleotide. *Nature* **425**, 419–423 (2003).
32. Dunn, T.A. *et al.* A novel role of myosin VI in human prostate cancer. *Am. J. Pathol.* **169**, 1843–1854 (2006).
33. Tavares, M., Rezlan, E., Vostroknoutova, I., Khouadja, H. & Mebazaa, A. New pharmacologic therapies for acute heart failure. *Crit. Care Med.* **36**, S112–S120 (2008).
34. Green, J.L. *et al.* The MTIP-myosin A complex in blood stage malaria parasites. *J. Mol. Biol.* **355**, 933–941 (2006).
35. Manstein, D.J. & Hunt, D.M. Overexpression of myosin motor domains in *Dictyostelium*: screening of transformants and purification of the affinity tagged protein. *J. Muscle Res. Cell Motil.* **16**, 325–332 (1995).
36. Margossian, S.S. & Lowey, S. Preparation of myosin and its subfragments from rabbit skeletal muscle. *Meth. Enzymol.* **85**, B55–B71 (1982).
37. Lehrer, S.S. & Kerwar, G. Intrinsic fluorescence of actin. *Biochemistry* **11**, 1211–1217 (1972).
38. Criddle, A.H., Geeves, M.A. & Jeffries, T. The use of actin labelled with N-(1-pyrenyl)iodoacetamide to study the interaction of actin with myosin subfragments and troponin/tropomyosin. *Biochem. J.* **232**, 343–349 (1985).
39. Agarwal, S. & Knölker, H.-J. A novel pyrrole synthesis. *Org. Biomol. Chem.* **2**, 3060–3062 (2004).
40. Furch, M., Geeves, M.A. & Manstein, D.J. Modulation of actin affinity and actomyosin adenosine triphosphatase by charge changes in the myosin motor domain. *Biochemistry* **37**, 6317–6326 (1998).

41. Batra, R., Geeves, M.A. & Manstein, D.J. Kinetic analysis of *Dictyostelium discoideum* myosin motor domains with glycine-to-alanine mutations in the reactive thiol region. *Biochemistry* **38**, 6126–6134 (1999).
42. Fujita-Becker, S. *et al.* Changes in Mg^{2+} ion concentration and heavy chain phosphorylation regulate the motor activity of a class I myosin. *J. Biol. Chem.* **280**, 6064–6071 (2005).
43. Fedorov, R., Witte, G., Urbanke, C., Manstein, D.J. & Curth, U. 3D structure of *Thermus aquaticus* single-stranded DNA-binding protein gives insight into the functioning of SSB proteins. *Nucleic Acids Res.* **34**, 6708–6717 (2006).
44. Brenner, B. Technique for stabilizing the striation pattern in maximally calcium-activated skinned rabbit psoas fibers. *Biophys. J.* **41**, 99–102 (1983).
45. Kraft, T. *et al.* Equilibration and exchange of fluorescently labeled molecules in skinned skeletal muscle fibers visualized by confocal microscopy. *Biophys. J.* **69**, 1246–1258 (1995).
46. Brenner, B. & Eisenberg, E. Rate of force generation in muscle: correlation with actomyosin ATPase activity in solution. *Proc. Natl. Acad. Sci. USA* **83**, 3542–3546 (1986).
47. Brenner, B. Effect of Ca^{2+} on cross-bridge turnover kinetics in skinned single rabbit psoas fibers: implications for regulation of muscle contraction. *Proc. Natl. Acad. Sci. USA* **85**, 3265–3269 (1988).
48. Edman, K.A. The velocity of unloaded shortening and its relation to sarcomere length and isometric force in vertebrate muscle fibres. *J. Physiol. (Lond.)* **291**, 143–159 (1979).
49. Brunger, A.T. *et al.* Crystallography & NMR system: a new software suite for macromolecular structure determination. *Acta Crystallogr. D Biol. Crystallogr.* **54**, 905–921 (1998).
50. Schmidt, M.W. *et al.* The general atomic and molecular electronic structure system. *J. Comput. Chem.* **14**, 1347–1363 (1993).